RSC Advances

PAPER

View Article Online
View Journal | View Issue

Cite this: *RSC Adv.*, 2026, **16**, 8499

Dynamic simulation study on gas flooding mechanism based on level set method at the micro–nano scale

Yi Yu,[a] Fei Wang, *[a] Xiaorong Guo,[a] Chaofan Chen,[a] Yuqian Wang[a] and Hailong Chen[b]

Gas flooding plays a crucial role in enhanced oil recovery; however, the underlying microscopic mechanisms, especially those related to interfacial changes, remain unclear. Based on a realistic geometric model of porous media, this study employs the level-set method to simulate the oil displacement processes of N_2 flooding, CO_2 immiscible flooding, CO_2 miscible flooding, and foam flooding at the microscale. The oil–gas interface is tracked throughout the simulations to compare and analyze the displacement behaviors of different gases. First, a dynamic simulation of the gas flooding process is conducted, analyzing the variations in pressure, velocity, and remaining oil volume fraction over time. Second, the effects of factors such as injection rate, foam gas–liquid ratio, and surface tension on oil displacement efficiency are investigated. Finally, the displacement performance of N_2 flooding, CO_2 flooding, and foam flooding is compared under specific conditions to examine the oil recovery mechanisms associated with different gases. The results indicate that the remaining oil volume fractions after N_2 flooding and CO_2 immiscible flooding are approximately 30%. Increasing the injection rate of N_2 and CO_2 can improve early-stage displacement performance and slightly enhance oil recovery. In contrast, the remaining oil volume fractions after CO_2 miscible flooding and foam flooding are about 10%. The optimal foam flooding effect is achieved at a gas–liquid ratio of 3 : 1 and a surface tension of 0.02, which corresponds to the lowest remaining oil volume fraction. Furthermore, the inlet pressure declines rapidly during N_2 and CO_2 immiscible flooding, resulting in a relatively low final pressure. In comparison, the inlet pressure decreases more gradually during CO_2 miscible flooding and foam flooding, maintaining a certain pressure level by the end of the process.

Received 30th December 2025
Accepted 5th February 2026

DOI: 10.1039/d5ra10088g

rsc.li/rsc-advances

Introduction

Oil is an important industrial energy source,[1–3] occupying an absolute dominant position in the fossil energy structure.[4,5] However, the distribution and development of the world's oil is highly unbalanced. There are many unconventional reservoirs such as low permeability, tight and heavy oil reservoirs that are difficult to exploit.[6] the reserves per unit area are small, and the quality of oil and gas resources is poor.[7] Their exploration and development are difficult.[8] At the same time, the primary and secondary exploitation of oilfields usually can only recover 30% to 40% of the geological reserves of oilfields,[9,10] and more than 60% of the crude oil remains underground[11] in the form of adsorption, residue, *etc.* Through gas flooding, chemical agent or thermal technology,[12,13] the tertiary recovery can change the crude oil viscosity, interfacial tension or rock wettability.[14] The recovery factor can be increased by 10–20% or even higher.[15] Therefore, the development of tertiary recovery technology is the key to improve oil recovery.[16] Among them, the gas flooding technology is widely used because it is easier to establish an effective flooding pressure system, improve the flooding conditions efficiently, have strong adaptability, wide application range, low cost and environmental protection properties.[17,18]

The gas injected into the oil layer diffuses and dissolves in the crude oil, and the interaction between gas, crude oil, rock and water can reduce the crude oil viscosity,[19–21] improve the crude oil recovery rate, maximize the development of underground remaining oil resources, extend the economic life of the oilfield, effectively reduce the production energy consumption of the oilfield,[22] and realize the emission reduction and permanent storage of greenhouse gases.[23] The gas injection and oil flooding technology has a variety of gas sources and flexible injection methods.[24] It is found that the types of gases that can be used for crude oil flooding include CO_2, N_2, flue gas, hydrocarbon gas, air and other mediums;[25,26] injection methods include vertical/horizontal well huff and

[a]*College of Electromechanical Engineering, Qingdao University of Science and Technology, Shandong, Qingdao, 266061, PR China. E-mail: wangfeiupc@163.com*
[b]*Oil & Gas Field Applied Chemistry Key Laboratory of Sichuan Province, Southwest Petroleum University, Sichuan, Chengdu, 610500, PR China*

puff, CO_2 miscible/immiscible flooding, water gas alternate flooding, foam flooding, *etc.*[27–29] The combination of different gas and injection methods makes the gas flooding operation flexible and diverse, and can adapt to the development of different geological structures and heavy oil reservoirs.[30,31] The research shows that in the process of gas injection and oil flooding, the gas diffuses into the crude oil under the effect of pressure and concentration gradient, dissolves in the crude oil, decomposes the heavier components in the crude oil into lighter components,[32] reduces the concentration and content of the heavier components, reduces the viscosity of the crude oil, improves the mobility of the oil, and improves the oil recovery.[33] Nowadays, gas flooding technology has been applied in many oilfields around the world on a large scale, greatly improving the oil recovery rate.

Gas flooding has good adaptability to many types of reservoirs, which is suitable for both medium and high permeability old oilfields and ultra-low permeability oilfields.[34] However, the technology of enhancing oil recovery through gas flooding still faces many problems.[35] The types and scale of reservoir gas injection tests are relatively small. At the nanoscale, the rules of oil and gas adsorption and flow are still unknown, and there are obvious differences from the macro scale.[36,37] For example, the permeability is very low, and the flow does not obey Darcy's law.[38] In the process of gas flooding, the changes of phase transition, interface dynamic evolution and remaining oil morphology with time are not clear,[39] especially considering the porous media flow process of oil–gas interface change,[40] which leads to the deviation of oil flooding mechanism cognition and restricts the large-scale application of gas flooding technology in industry.[41] Therefore, the study of the flow state of crude oil and the interaction mechanism between gas and crude oil in the micro nano channel is the theoretical basis for the development of CO_2 and other gases to improve oil and gas recovery technology.[42]

Therefore, based on the real geometric structure model of porous media, this study establishes a porous media gas flooding model, uses the level set method to simulate the oil flooding process of N_2 flooding, CO_2 immiscible flooding, CO_2 miscible flooding and foam flooding at the micro scale, tracks the oil–gas interface, explores the influence of injection rate, gas–liquid ratio of foam, surface tension and other factors on oil flooding effect, and compares and analyzes the flooding effect and oil flooding law of different gases under the same conditions. The results of this paper can enrich the theory of gas flooding and provide guidance for the application of gas flooding.

Simulation and analysis methods

Establishment of porous media model and mesh generation

Fig. 1(a) shows the geometric model of porous media used in the simulation, which is designed according to the image of real core slice scanning,[43,44] and the model size is 640 μm × 320 μm. As shown in Fig. 1(b), free triangle mesh is used for mesh generation by using the finite element method.

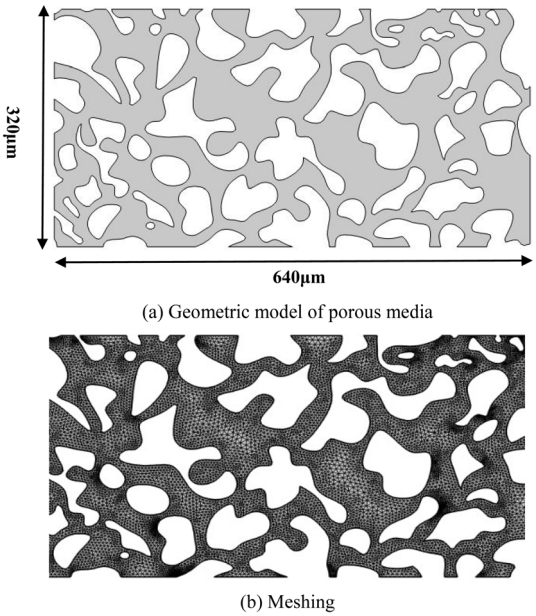

(a) Geometric model of porous media

(b) Meshing

Fig. 1 Establishment of porous media model.

Establishment of mathematical model based on level set method

The fluid interface is represented by the contour of the level set function $\phi = 0.5$. In gas, $\phi = 0$, in oil, $\phi = 1$. Therefore, the level set function can be regarded as the volume fraction of oil. The migration of the fluid interface separating the two phases is as follows:

$$\frac{\partial \phi}{\partial t} + u \cdot \nabla \phi = \gamma \nabla \cdot \left(\varepsilon \nabla \phi - \phi(1-\phi) \frac{\nabla \phi}{|\nabla \phi|} \right) \quad (1)$$

The ε parameter determines the thickness of the interface. When using the numerical stability method for the level set equation, it is usually possible to specify the interface thickness as $\varepsilon = hc/2$, where hc is the size of the characteristic grid in the region transferred through the interface (based on our model, $hc \approx 5$ μm). The γ parameter determines the number of reinitialization. An appropriate γ value is the maximum speed in the model (in our simulation, $\gamma = 0.1$). The multi physical field coupling characteristics define the density and viscosity according to the following formula:

$$\rho = \rho_{gas} + (\rho_{oil} - \rho_{gas})\phi \quad (2)$$

$$\mu = \mu_{gas} + (\mu_{oil} - \mu_{gas})\phi \quad (3)$$

Among them, gas represents N_2, CO_2, CO_2 miscible and foam.

According to the above formula definition, the density and viscosity coefficient change smoothly at the fluid interface. The δ function can be approximated as:

$$\delta = 6|\phi(1-\phi)||\nabla \phi| \quad (4)$$

The interface normal can be calculated according to the following equation:

$$n = \frac{\nabla\phi}{|\nabla\phi|} \tag{5}$$

This model is based on the Navier Stokes equation of incompressible fluid to simulate the mass and momentum transfer of fluid. The Navier Stokes equation with surface tension is:

$$\rho\frac{\partial u}{\partial t} + \rho(u\cdot\nabla)u = \nabla\cdot\left[-pI + \mu\left(\nabla u + (\nabla u)^{\mathrm{T}}\right)\right] + F_{\mathrm{st}} + \rho g$$
$$\nabla\cdot u = 0 \tag{6}$$

where, μ is equal to the dynamic viscosity (N s m^{-2}), ρ is the density (kg m^{-3}), u is the viscosity (m s^{-1}), p is the pressure (Pa), F_{st} is the surface tension acting on the gas/oil interface, and g is the gravity vector (m s^{-2}). The surface tension calculation equation is:

$$F_{\mathrm{st}} = \sigma\delta\kappa n \tag{7}$$

where, σ is the surface tension (N m^{-1}), n is the interface normal, $\kappa = -\nabla\cdot n$ is the curvature, and δ is a Dirac function, which is non-zero only at the fluid interface.

Establishment and parameter setting of different gas flooding models

The inlet and outlet are selected as shown in Fig. 2 below. The boundary condition is velocity, normal inflow velocity U_0; the static pressure at the outlet $P_0 = 0$ Pa. The two fluids are oil and gas respectively. Surface tension $\sigma = 0.02$ N m^{-1}. The dynamic viscosity is 0.1 Pa s. In the subsequent analysis, a point at the inlet is selected as the base point of pressure analysis to analyze the pressure change during fluid injection.

At the beginning, the porous medium is filled with oil, the density of the oil is 800 kg m^{-3}, the dynamic viscosity is 0.1 Pa s, and the gas is injected at the entrance of the porous medium. The gas injection rate is set at 0.001 m s^{-1}, and the foam gas–liquid ratio is 4 : 1. The oil flooding process of different kinds of gas is simulated respectively, and the fluid velocity diagram, pressure diagram and residual oil volume fraction diagram at different times are obtained. Based on the results, the laws and characteristics of different gas flooding are analyzed.

In the process of N_2 and CO_2 flooding, the gas injection rate has a great impact on gas flooding. Therefore, this study will add two groups of gas flooding simulation, keep other initial conditions unchanged, only change the gas injection rate, set the gas injection rate as 0.003 m s^{-1} and 0.005 m s^{-1}, and explore the influence of gas injection rate on gas flooding.

In the process of foam flooding, the gas–liquid ratio and surface tension of foam have a great impact on foam flooding. Therefore, in the foam flooding simulation, this study will use the control variable method to change the gas–liquid ratio and surface tension of foam, and explore the influence of the gas–liquid ratio and surface tension of foam on foam flooding. With other initial conditions unchanged, two sets of simulations with gas–liquid ratio of 3 : 1 and 1 : 1 were added to explore the effect of gas–liquid ratio of foam on foam flooding; with other initial conditions unchanged, two groups of studies with surface tension of 0.01 N m^{-1} and 0.03 N m^{-1} were added to explore the effect of surface tension on foam flooding.

At the same time, the effects of different gas flooding are also different, so this study will compare different gas flooding under the same conditions, set the gas injection rate to be 0.001 m s^{-1}, the surface tension to be 0.02 N m^{-1}, and the foam gas–liquid ratio to be 4 : 1, get the pressure, velocity and remaining oil volume fraction change curves of different gas flooding, and compare the oil flooding effects of different gas flooding.

The basic physical parameters of the fluid used in this simulation are as follows (Table 1).[45–49]

Based on the above settings, we use COMSOL software to carry out relevant simulation research.

Table 1 Physical parameters of fluids[a]

Fluids	Density (kg m^{-3})	Viscosity (Pa s)	Interfacial tension (N m^{-1})
N_2	20	0.02	0.02
CO_2 immiscible	400	0.03	0.02
CO_2 miscible	700	0.05	0.00003 (almost 0)
Foam	200	0.04	0.01
Oil	800	0.1	0.02

[a] The parameters of different fluids are taken according to the displacement environment under different temperature and pressure. For example, the temperature and pressure conditions corresponding to CO_2 miscible and immiscible must be different. This simulation is not specific to specific reservoir conditions, but only compares the different displacement effects due to different fluid properties.

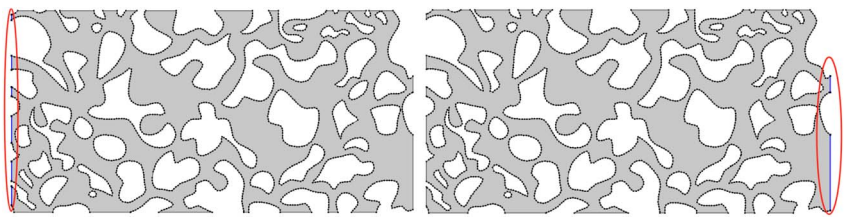

Fig. 2 Setting of baseline initial boundary value conditions.

Results and discussion

Analysis of N_2 flooding results

The nitrogen injection rate at the inlet of porous medium is 0.001 m s^{-1}, the density of oil is 800 kg m^{-3}, the dynamic viscosity is 0.1 Pa s, and the surface tension is 0.02 N m^{-1}. The dynamic simulation is carried out according to the geometric model and initial settings above, and the pressure diagram and fluid velocity diagram at t = 1, 2, 3 and 4 s are obtained as follows (Fig. 3):

The simulation results show that the average pressure is the maximum when the gas is just injected into the porous medium, and the average pressure gradually decreases as the gas gradually enters the porous medium. At different times, the pressure is the maximum near the inlet and the minimum near the outlet. The fluid velocity distribution is relatively uniform at different times, and the fluid flow velocity is large in the middle narrow channel. The volume fraction of remaining oil can reflect the efficiency of gas flooding. The distribution of remaining oil at different times during nitrogen flooding is shown in Fig. 4.

It can be seen from the distribution of remaining oil in Fig. 4 that as the oil flooding process proceeds, the oil is continuously displaced out of the porous media, and finally there is a part of residual oil in the model, which is concentrated in the upper right and lower right of the model. There is almost no residual oil in the first third of the model, and the oil in the channel with the fastest fluid flow rate is completely displaced.

Under the condition of keeping other initial conditions unchanged, change the nitrogen injection rate, and add two groups of simulations with nitrogen injection rates of 0.003 m s^{-1} and 0.005 m s^{-1} to explore the impact of nitrogen injection rate on nitrogen flooding. The simulation results at the same time are shown in Fig. 5. It can be seen from the

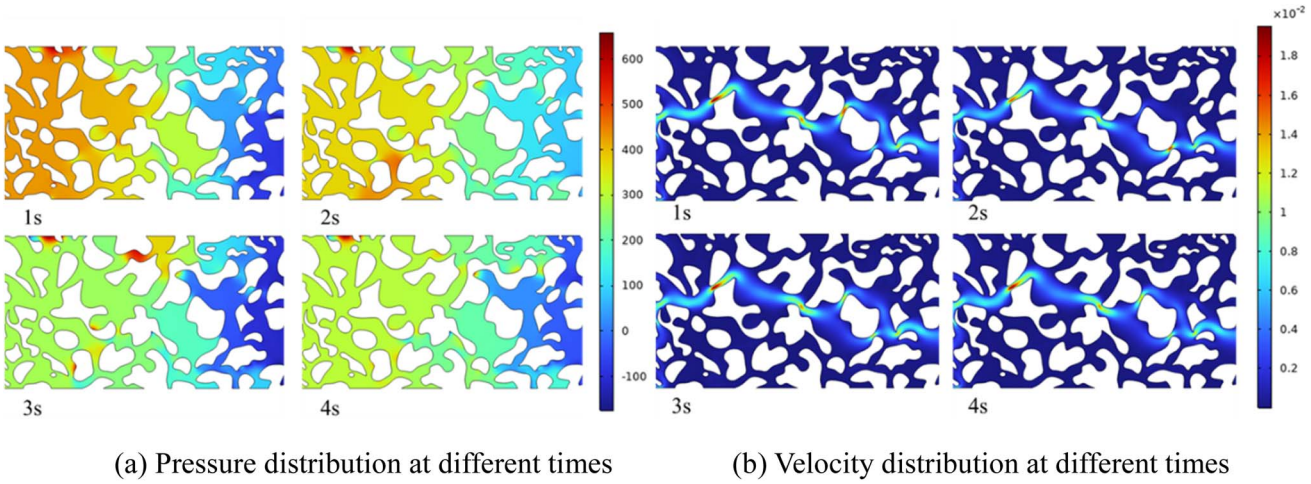

Fig. 3 Pressure and velocity distribution of nitrogen flooding at different times.

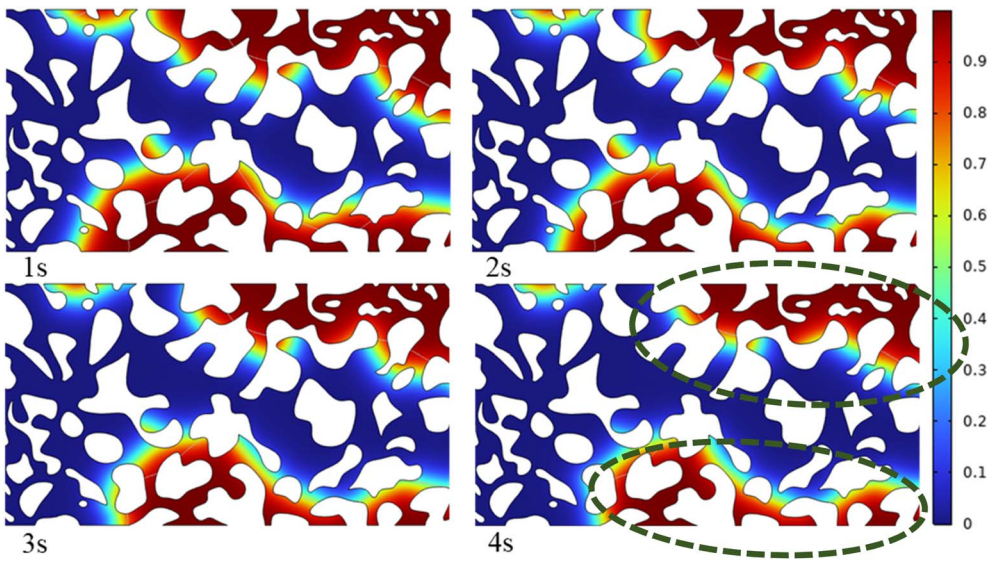

Fig. 4 Volume fraction of remaining oil.

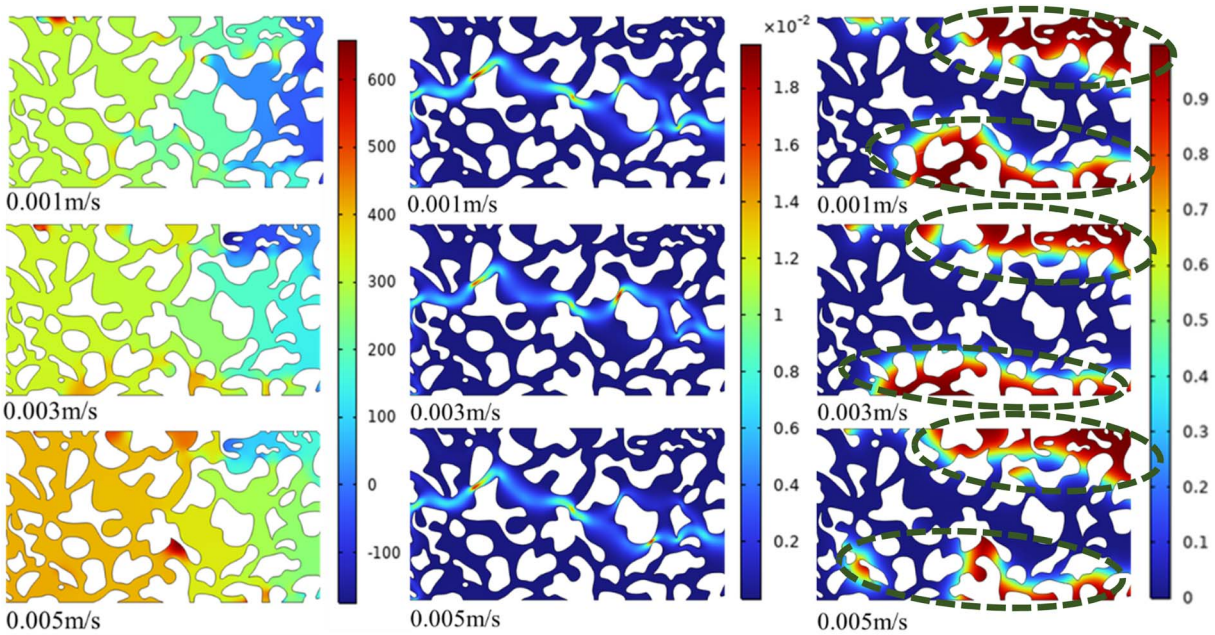

Fig. 5 Pressure, velocity and remaining oil changes at the same time at different injection rates.

simulation results that at different nitrogen injection rates, the pressure of the model is the largest at the gas inlet. As nitrogen enters the model, it becomes smaller and smaller. The distribution of fluid velocity in the model is relatively uniform, and the flow rate is large in the middle narrow channel. At the end of the oil flooding process, the remaining oil is concentrated in the upper right and lower right of the model. With the increase of nitrogen injection rate, the overall pressure and fluid flow velocity increased at the same time, and it can be found that increasing the nitrogen injection rate can slightly increase the oil recovery.

It can be seen from Fig. 6 that with the increase of nitrogen injection rate, the inlet pressure increases significantly, but it will eventually approach 0 kPa. When the nitrogen injection rate is 0.001 m s^{-1}, the pressure drop rate is the slowest with the oil flooding process. When the nitrogen injection rate is 0.005 m s^{-1}, the pressure drop rate is the fastest with the oil flooding process. It can be seen that within a certain range, with the continuous increase of nitrogen injection rate, the inlet pressure drop rate will continue to increase.

As can be seen from Fig. 7, when the nitrogen injection rate is 0.001 m s^{-1}, the volume fraction of remaining oil is the largest, the flooding effect is the worst, and the volume fraction of remaining oil is close to 0.27. When the nitrogen injection rate is 0.005 m s^{-1}, the volume fraction of remaining oil is close to 0.15. It can be seen that within a certain range, the oil flooding effect will gradually increase with the increase of nitrogen injection rate. At the same time, it can be seen that

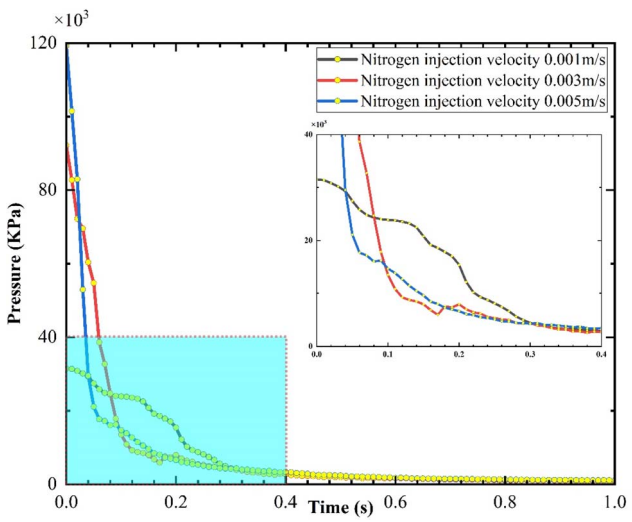

Fig. 6 Pressure change at different injection rates.

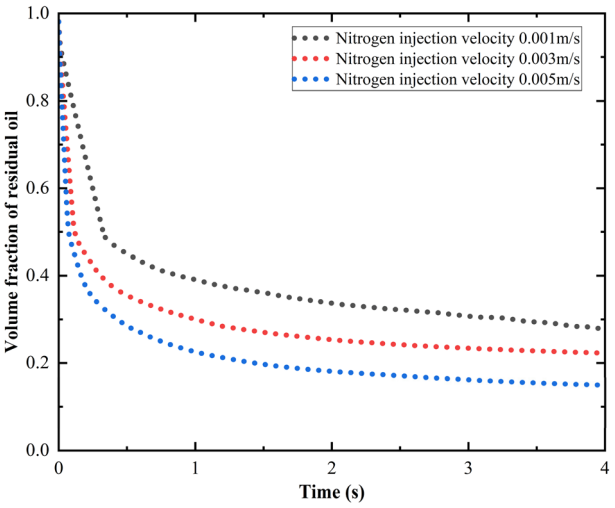

Fig. 7 Variation of residual oil volume fraction at different injection rates.

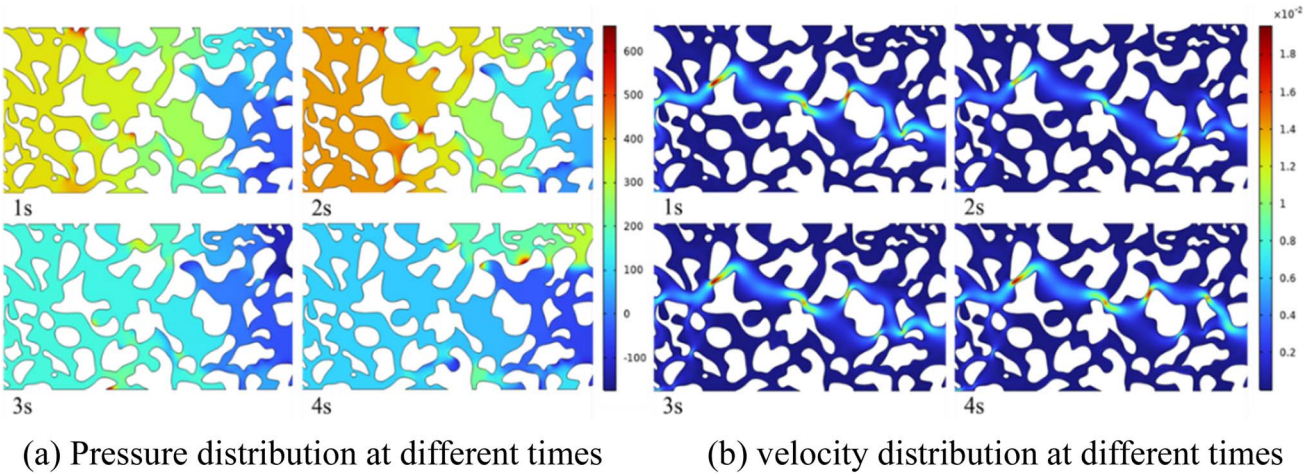

Fig. 8 Pressure and velocity distribution of CO_2 immiscible flooding at different times.

when the nitrogen injection rate is 0.005 m s^{-1}, the volume fraction of remaining oil decreases the fastest and the oil flooding speed is the fastest. When the nitrogen injection rate is 0.001 m s^{-1}, the remaining oil volume fraction decreases the slowest and the oil flooding speed is the slowest. Therefore, increasing the nitrogen injection rate can obtain better early oil flooding effect and greater recovery.

Analysis of CO_2 flooding results

(1) CO_2 immiscible flooding result analysis. The CO_2 injection rate at the entrance of porous medium is 0.001 m s^{-1}, the density of oil is 800 kg m^{-3}, the dynamic viscosity is 0.1 Pa s, and the surface tension is 0.02 N m^{-1}. The dynamic simulation is carried out according to the geometric model and initial settings above, and the pressure diagram and fluid velocity diagram at $t = 1$, 2, 3 and 4 s are obtained as shown in Fig. 8.

According to the simulation results, the pressure presents a state of high pressure near the inlet and outlet and low pressure near the outlet. At the beginning, the overall pressure is the maximum. With the injection of carbon dioxide, the overall pressure continues to decline. The fluid flow velocity distribution is relatively uniform, and the flow velocity is larger in the narrow channel in the middle of the porous media model. The remaining oil distribution of CO_2 immiscible flooding at different times is shown in Fig. 9.

It can be seen from Fig. 9 that as the oil flooding process proceeds, carbon dioxide gas continuously enters the pores of porous media, and oil is continuously displaced. Finally, the volume fraction of remaining oil in the first third of the model area is basically zero, and the remaining oil is concentrated in the upper and lower middle right areas of the model.

Keep other initial conditions unchanged, only change the CO_2 injection rate, and add two sets of simulations with CO_2 injection rates of 0.003 m s^{-1} and 0.005 m s^{-1} to explore the impact of CO_2 immiscible injection rate on CO_2 gas flooding. The simulation results at the same time are shown in Fig. 10

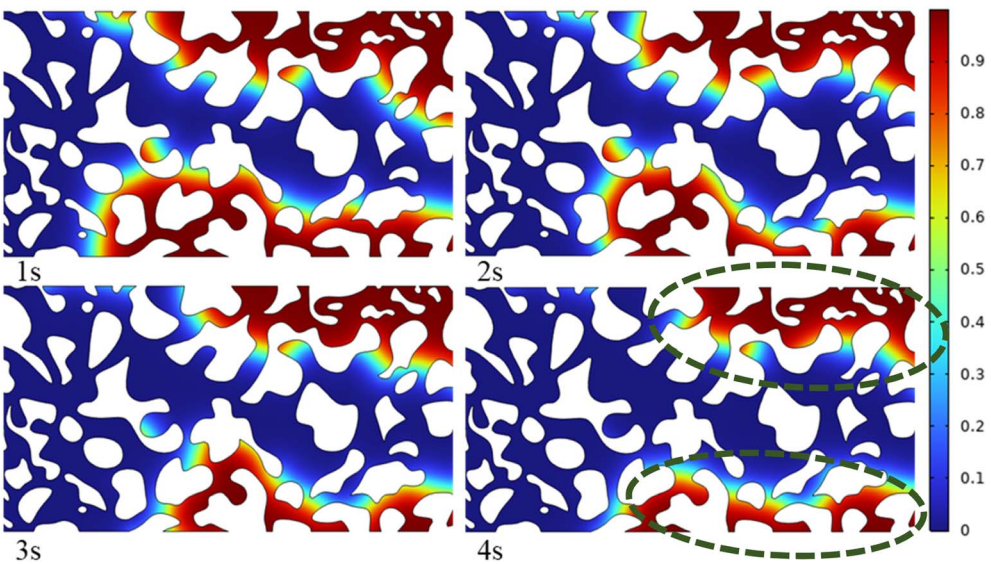

Fig. 9 Volume fraction of remaining oil.

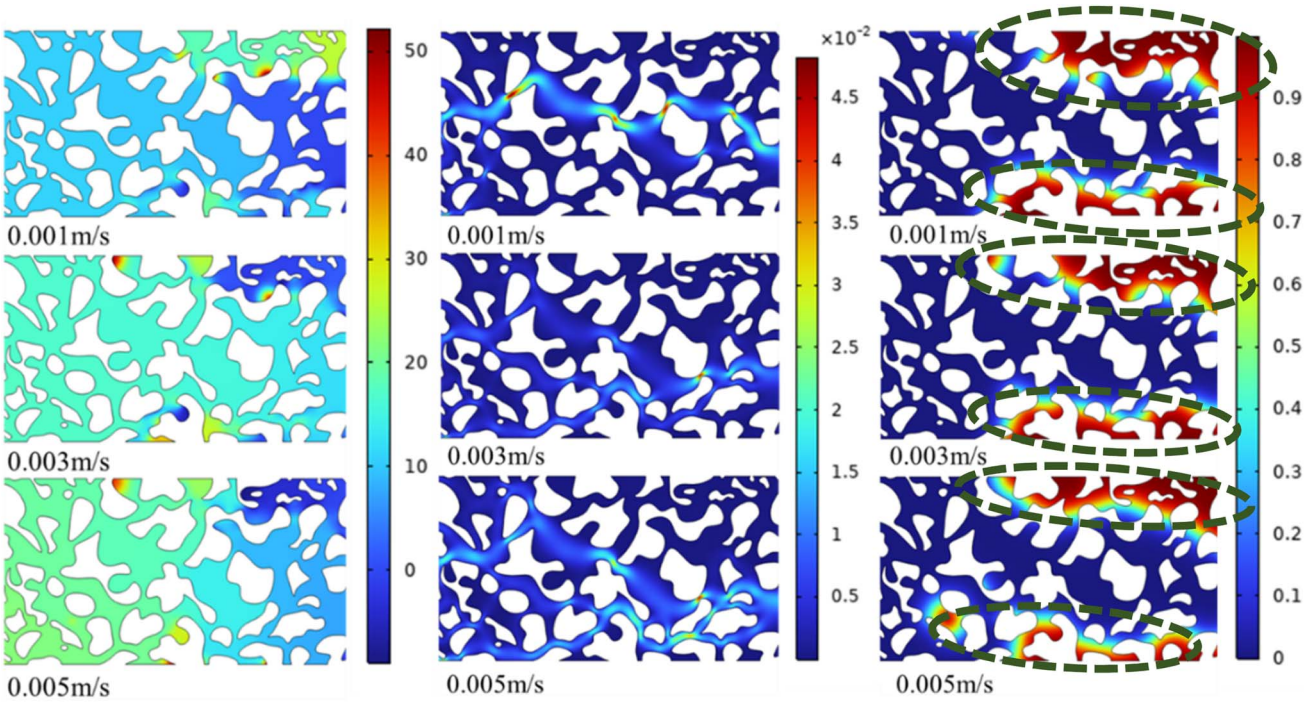

Fig. 10 Effect of velocity on CO_2 immiscible flooding.

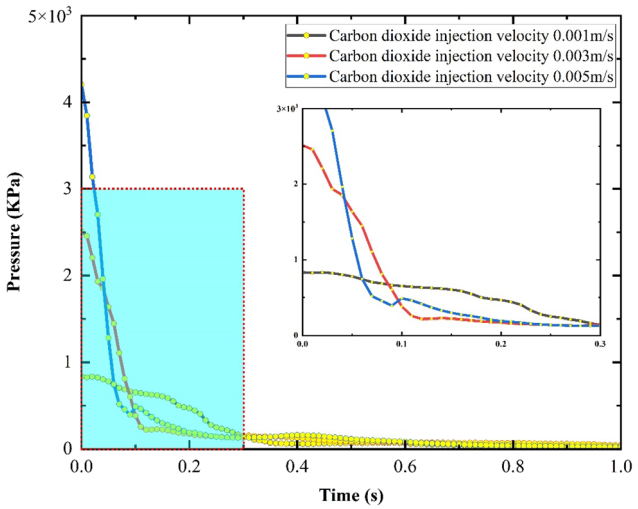

Fig. 11 Pressure change at different injection rates.

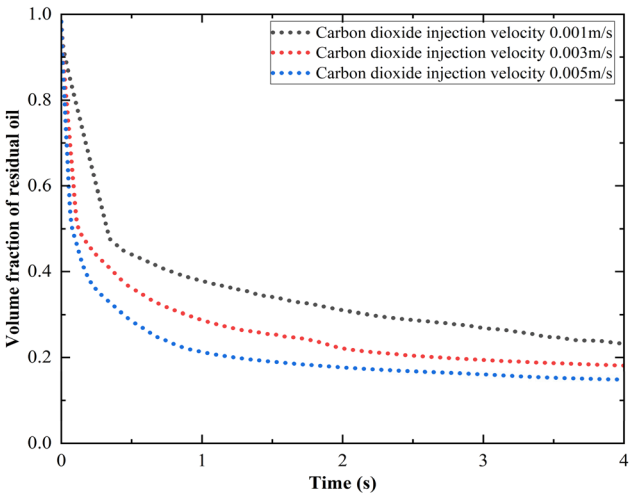

Fig. 12 Variation of residual oil volume fraction at different injection rates.

below. The influence of gas injection rate on CO_2 immiscible flooding was explored by changing the injection rate of CO_2. According to the simulation results, the pressure gradually decreases from the maximum at the inlet at different CO_2 injection rates, and the fluid flow velocity is evenly distributed in the channel, and the velocity is larger in some narrow channels. At the end of the oil flooding process, the volume fraction of remaining oil is similar. The remaining oil is distributed in the upper and lower parts of the middle right of the model, and the first third of the oil in the model is basically displaced out of the pore. With the increase of CO_2 injection rate, the average pressure increases, the fluid velocity in the model increases, the final remaining oil body integral decreases slightly, and the recovery factor increases slightly.

It can be seen from Fig. 11 that at different CO_2 injection rates, the pressure at this point at the inlet generally tends to decrease with the oil flooding process, and finally approaches a certain value without significant change. When the CO_2 injection rate is 0.001 m s^{-1}, the inlet pressure at this point is the minimum at the beginning. When the CO_2 injection rate is 0.005 m s^{-1}, the inlet pressure is the maximum at 0 s. It can be seen that within a certain range, with the continuous increase of

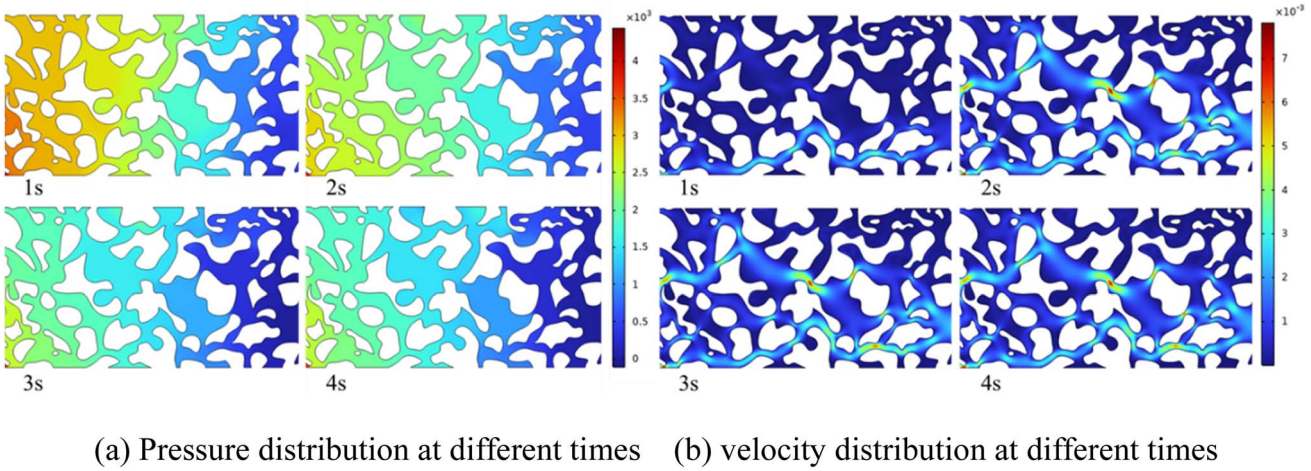

Fig. 13 Pressure and velocity distribution of CO_2 miscible flooding at different times.

CO_2 injection rate, the inlet pressure will continue to rise. When the CO_2 injection rate is 0.001 m s^{-1}, the pressure drop rate is the slowest with the oil flooding process. When the CO_2 injection rate is 0.005 m s^{-1}, the pressure drop rate is the fastest with the oil flooding process. It can be seen that within a certain range, with the continuous increase of CO_2 injection rate, the inlet pressure drop rate will continue to increase.

It can be seen from Fig. 12 that when the CO_2 injection rate is 0.001 m s^{-1}, the volume fraction of remaining oil is the largest and the flooding effect is the worst, with the volume fraction of remaining oil about 0.23. When the CO_2 injection rate is 0.005 m s^{-1}, the residual oil volume fraction is the smallest, and the flooding effect is the best, and the residual oil volume fraction is about 0.16. At the same time, it can be seen that when the CO_2 injection rate is 0.005 m s^{-1}, the volume fraction of remaining oil decreases the fastest and the oil flooding speed is the fastest. When the CO_2 injection rate is 0.001 m s^{-1}, the remaining oil volume fraction decreases the slowest and the oil flooding speed is the slowest. It can be seen that in a certain range, increasing the injection rate of CO_2 can effectively improve the oil recovery and oil flooding rate.

(2) CO_2 miscible flooding result analysis. The CO_2 miscible injection rate at the entrance of porous medium is 0.001 m s^{-1}, the density of oil is 800 kg m^{-3}, the dynamic viscosity is 0.1 Pa s, and the surface tension is 0.02 N m^{-1}. The dynamic simulation is carried out according to the geometric model and initial settings above, and the pressure diagram and fluid velocity diagram at $t = 1$, 2, 3 and 4 s are obtained as shown in Fig. 13.

From the simulation results, it can be seen that the pressure in a small part of the area at the lower left corner of the model is the largest, and the pressure gradually decreases from the maximum at the inlet at different times, and the average pressure of the model becomes smaller and smaller as the oil

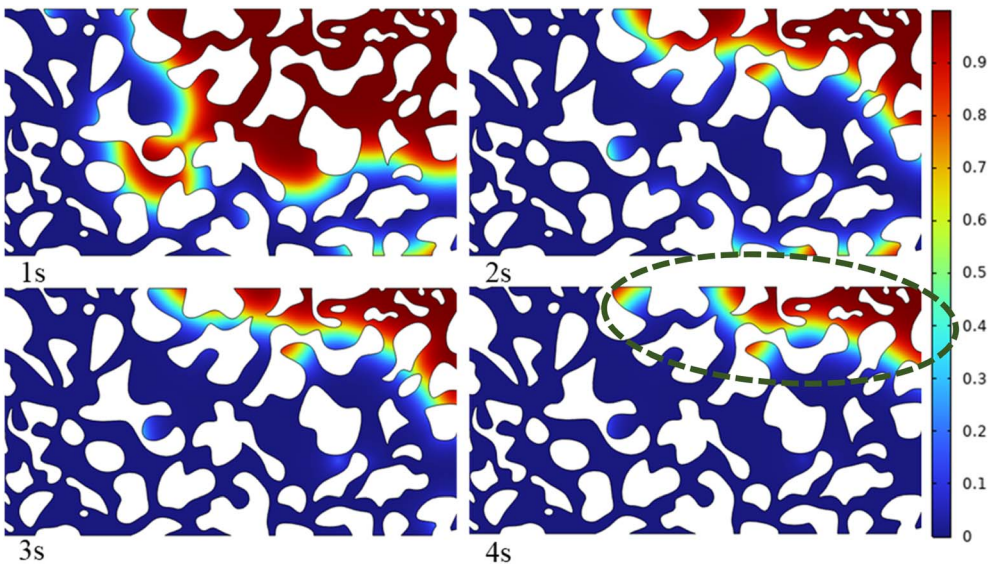

Fig. 14 Volume fraction of remaining oil.

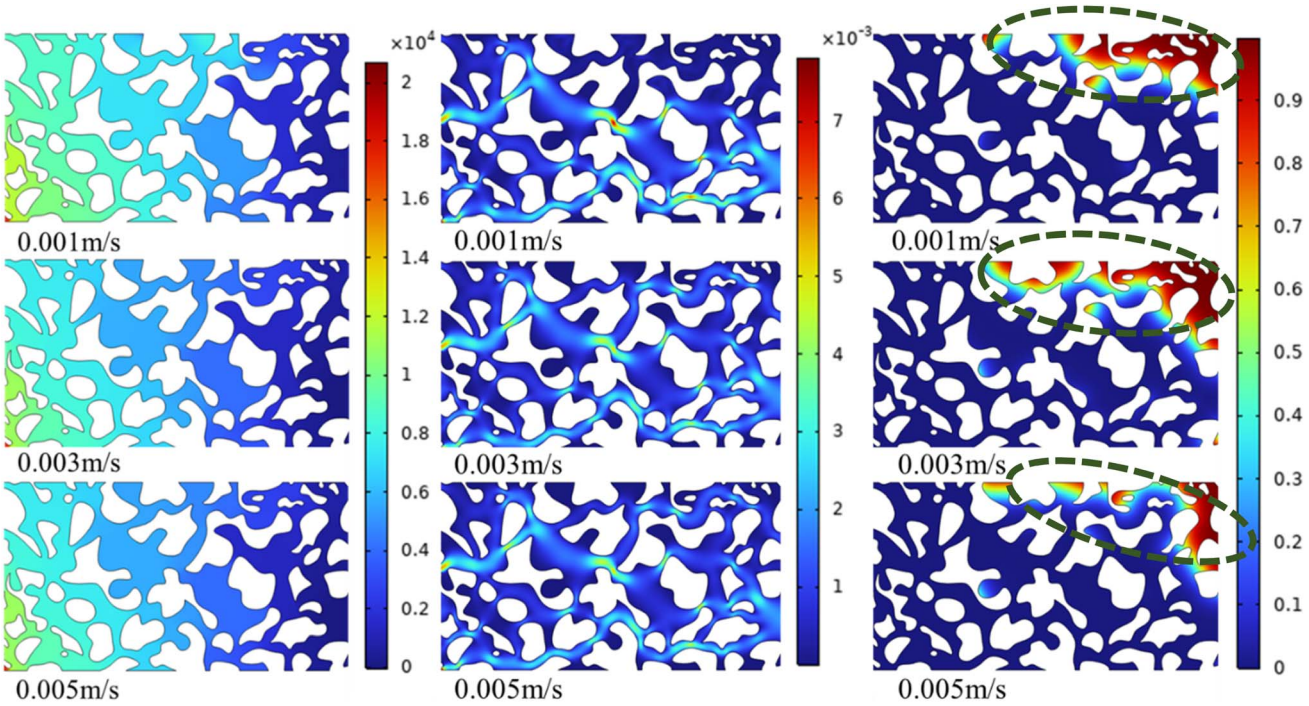

Fig. 15 Effect of velocity on CO_2 miscible flooding.

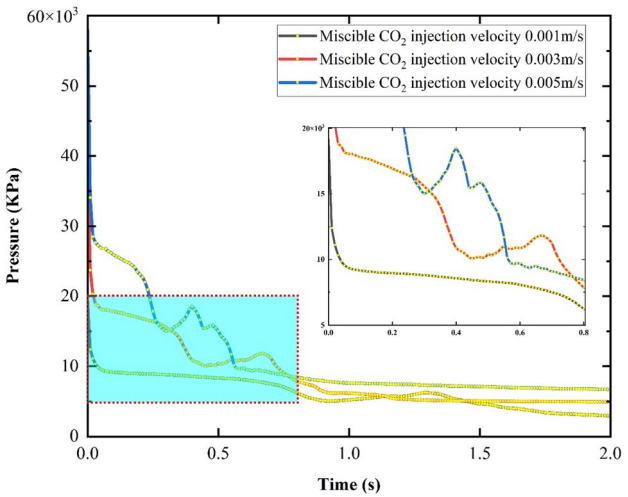

Fig. 16 Pressure change at different injection rates.

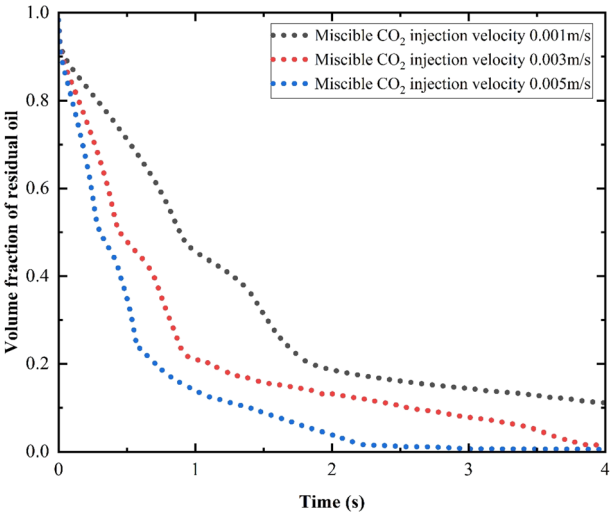

Fig. 17 Variation of residual oil volume fraction at different injection rates.

flooding process proceeds. The fluid flow velocity in the narrow channel of the porous media model is higher than that in other regions.

Fig. 14 shows the change of residual oil volume fraction during CO_2 miscible flooding.

According to the simulation results, with the oil flooding process, the oil in the lower part of the model and near the inlet part is first displaced out of the porous media model. After the oil flooding process is completed, the oil in the upper right part of the model is still left in the channel and has not been displaced, and the volume fraction of the remaining oil in other parts is close to zero.

Keep other initial conditions unchanged, only change the injection rate of miscible CO_2, and add two groups of simulations with miscible CO_2 injection rate of 0.003 m s^{-1} and 0.005 m s^{-1} to explore the impact of CO_2 miscible injection rate on gas flooding, and the simulation results at the same time are shown in Fig. 15.

According to the calculation results, it can be seen that the overall pressure distribution and pressure are basically the

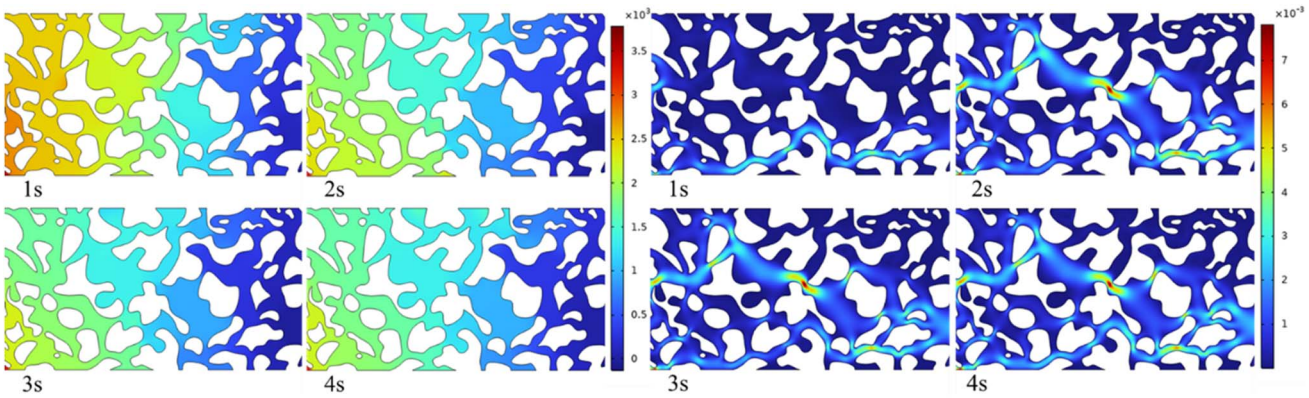

Fig. 18 Pressure and velocity distribution of foam flooding at different times.

same at the same time when the gas injection speed is increased, and the pressure is the largest in a small part of the area at the lower left corner of the model. The fluid flow velocity distribution is basically the same, and the velocity in the narrow channel is larger than that in other regions, but with the increase of gas injection velocity, the fluid flow velocity in the model also increases. The remaining oil in the model is distributed in the upper right area. When the gas injection rate increases, the oil recovery can be slightly increased.

It can be seen from Fig. 16 that at different miscible CO_2 injection rates, the pressure at this point at the inlet generally decreases with the oil flooding process, and finally approaches a certain value without significant change. When the injection rate of mixed phase is 0.001 m s^{-1}, the pressure at this point at the inlet is the minimum at the beginning. When the injection rate of miscible CO_2 is 0.005 m s^{-1}, the inlet pressure is the maximum at the beginning. It can be seen that within a certain range, the inlet pressure will continue to rise with the increasing injection rate. When the injection rate is 0.001 m s^{-1}, the pressure drop rate is the slowest with the oil flooding process. When the injection rate is 0.005m s^{-1}, the pressure drop rate is the fastest with the oil flooding process. It can be seen that within a certain range, with the continuous increase of miscible CO_2 injection rate, the inlet pressure drop rate will continue to increase in the process of oil flooding.

It can be seen from Fig. 17 that when the injection rate of miscible CO_2 is 0.001 m s^{-1}, the volume fraction of remaining oil is the largest and the flooding effect is the worst, with the volume fraction of remaining oil about 0.1. When the injection rate is 0.005 m s^{-1}, the residual oil volume fraction is the smallest, and the flooding effect is the best, and the residual oil volume fraction is about 0.013. At the same time, it can be seen that when the injection rate is 0.005 m s^{-1}, the volume fraction of remaining oil decreases the fastest and the oil

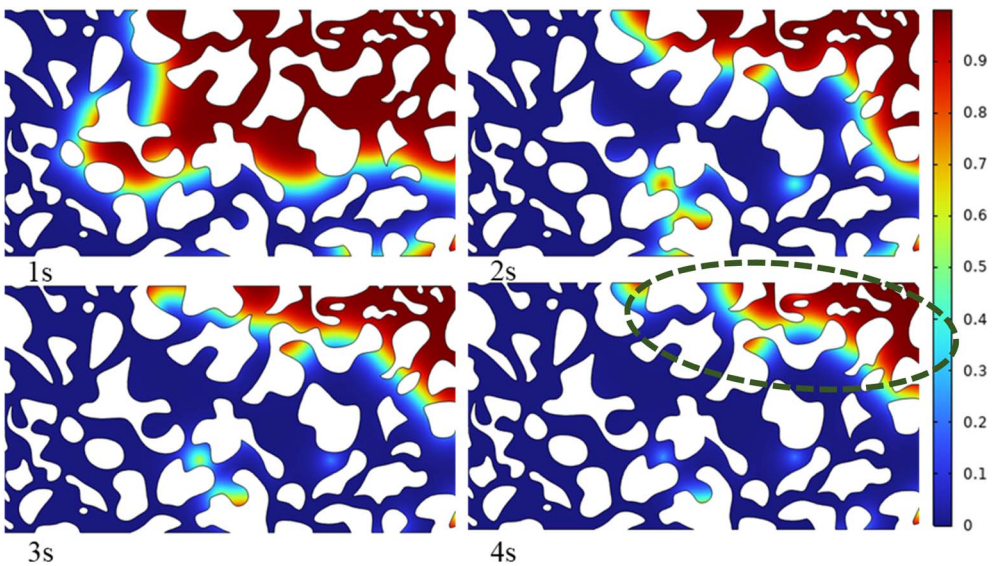

Fig. 19 Volume fraction of remaining oil.

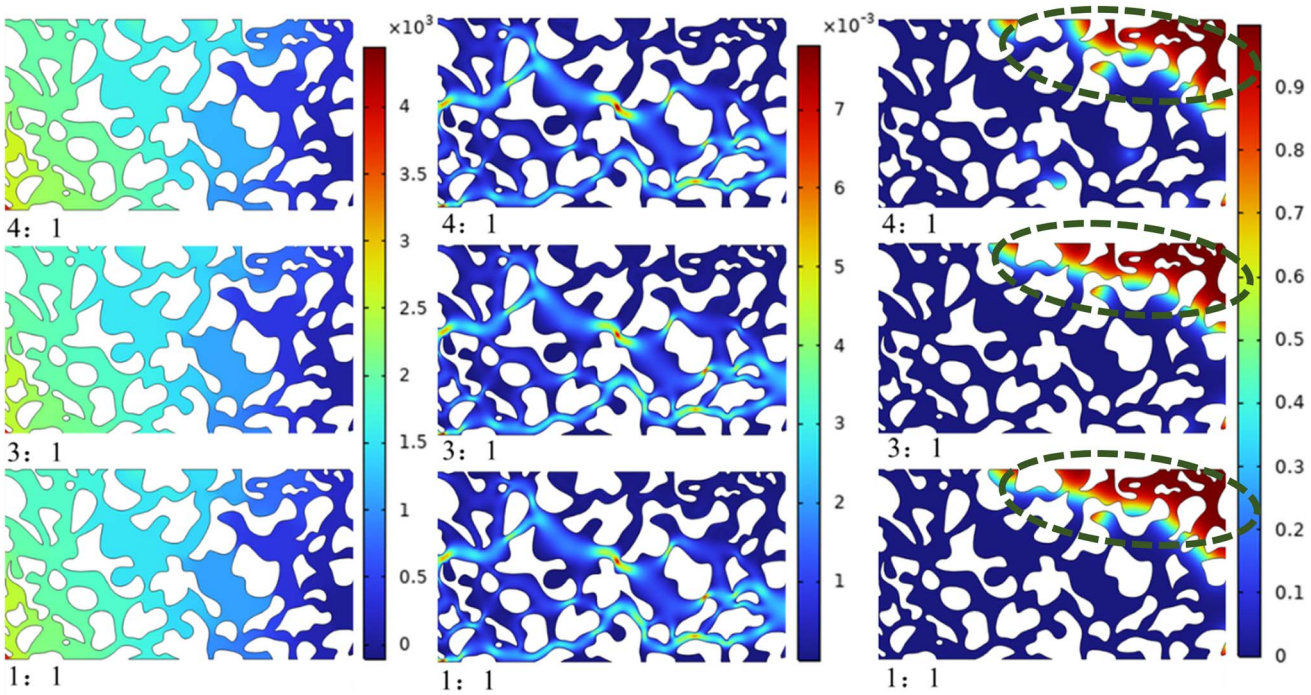

Fig. 20 Effect of gas–liquid ratio on foam flooding.

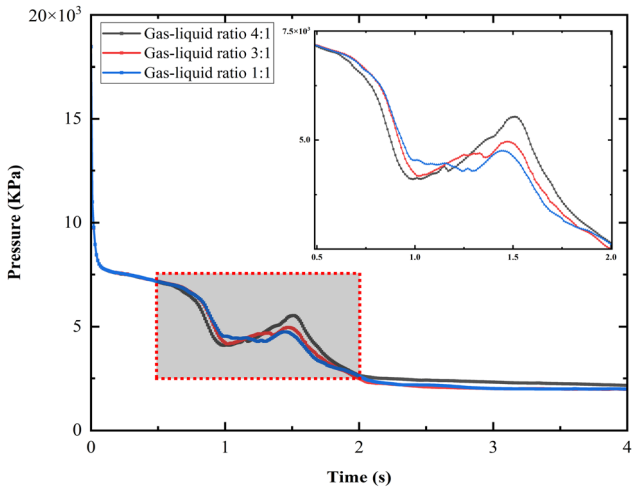

Fig. 21 Pressure change at different gas–liquid ratios.

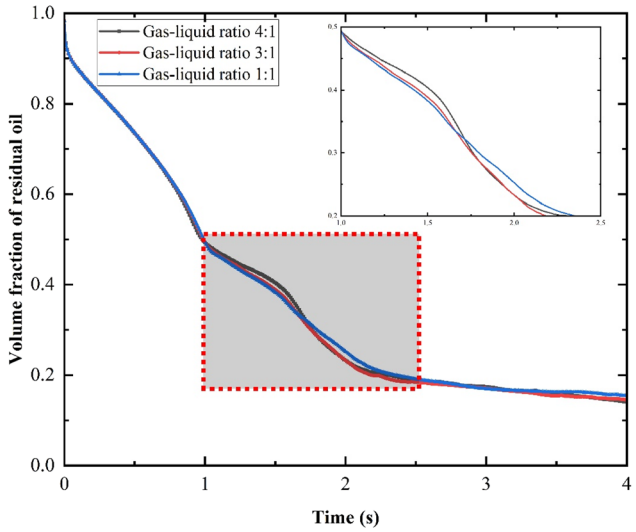

Fig. 22 Variation of residual oil volume fraction at different gas–liquid ratios.

flooding speed is the fastest. When the injection rate is 0.001 m s^{-1}, the remaining oil volume fraction decreases the slowest and the oil flooding speed is the slowest. It can be seen that in a certain range, increasing the injection rate of miscible CO_2 can effectively improve oil recovery and oil flooding rate.

Analysis of foam flooding results

The foam injection rate at the entrance of porous media is 0.001 m s^{-1}. The density of the oil is 800 kg m^{-3} and the dynamic viscosity is 0.1 Pa s. The density of foam is 200 kg m^{-3} (gas–liquid ratio is 4 : 1), and the dynamic viscosity is 0.04 Pa s. The surface tension is 0.01 N m^{-1}. Carry out dynamic simulation according to the above geometric model and initial settings. The pressure diagram and fluid velocity diagram at t = 1, 2, 3 and 4 s are obtained as shown in Fig. 18 below.

According to the pressure distribution diagram at different times, the pressure near the inlet is large, and the pressure near the outlet is small. With the oil flooding process, the overall pressure of the model gradually decreases. The velocity distribution of fluid flow is relatively uniform and larger in some narrow channels.

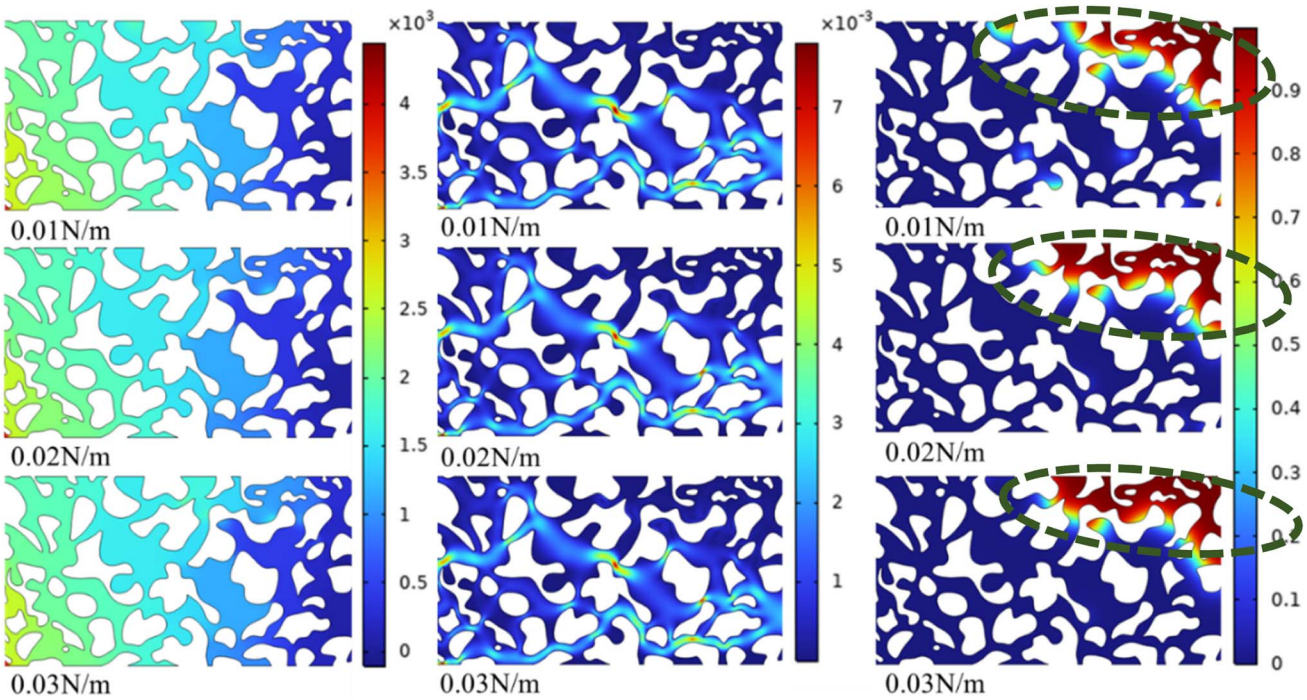

Fig. 23 Effect of surface tension on foam flooding.

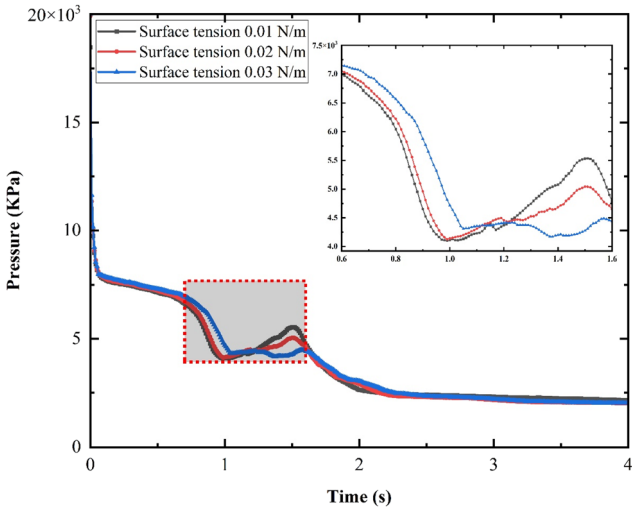

Fig. 24 Pressure change under different surface tension.

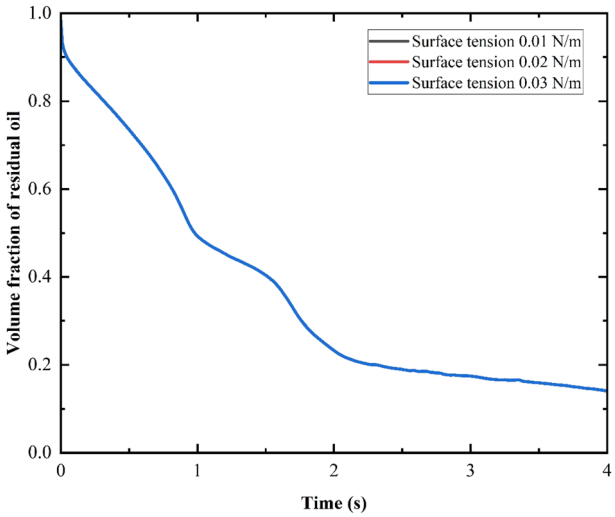

Fig. 25 Variation of residual oil volume fraction under different surface tension.

Fig. 19 shows the distribution change of remaining oil during oil flooding. As foam is injected from the inlet, the oil near and below the inlet of the model is first displaced out of the pores. As the oil flooding process proceeds, the oil is continuously displaced out of the porous media, and finally there is a part of residual oil in the model, which is concentrated in the upper right corner and upper middle part of the model, and the residual oil in other parts of the model is almost zero.

Under the condition that other initial conditions remain unchanged, the gas–liquid ratio is changed for comparative simulation analysis. Under the initial conditions, add two groups of models to change the foam gas–liquid ratio, that is, change the density of the material foam to 250 kg m^{-3} (gas–liquid ratio 3 : 1) and 500 kg m^{-3} (gas–liquid ratio 1 : 1). Oil flooding simulation was conducted for the three models to explore the influence of gas–liquid ratio of foam on foam oil flooding. The calculation results are shown in Fig. 20 below.

The simulation results show that the overall pressure and fluid flow velocity distribution and size are basically the same when foam flooding is carried out with different gas–liquid ratios. The pressure decreases gradually from the maximum near the inlet. The fluid flow velocity distribution is uniform, and the flow velocity is large in some narrow channels. From the

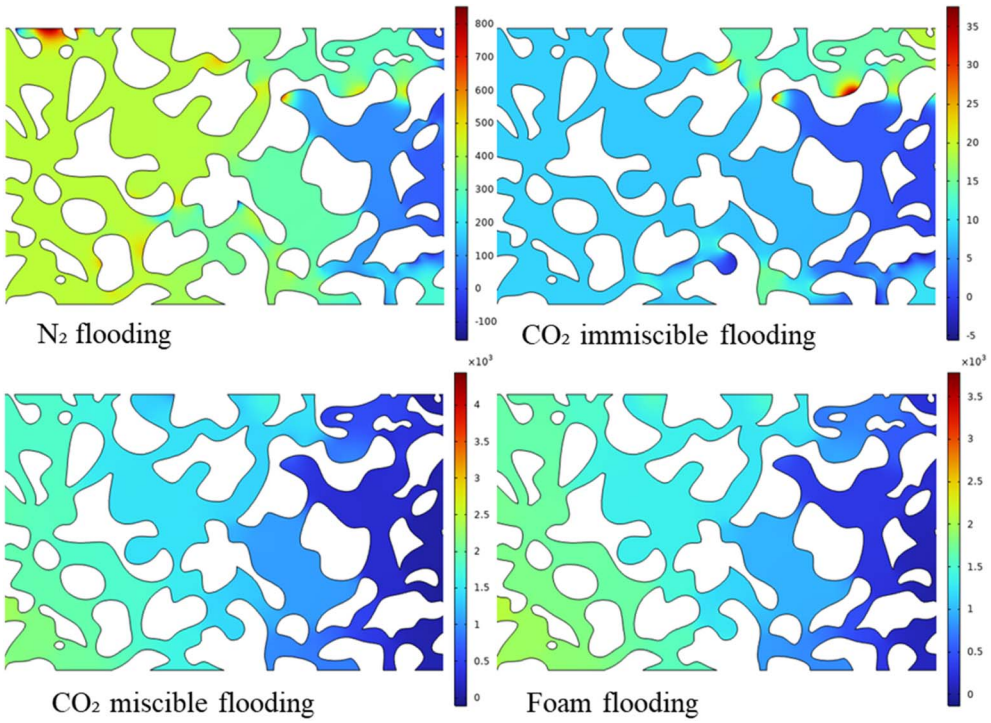

Fig. 26 Pressure distribution with different gas flooding.

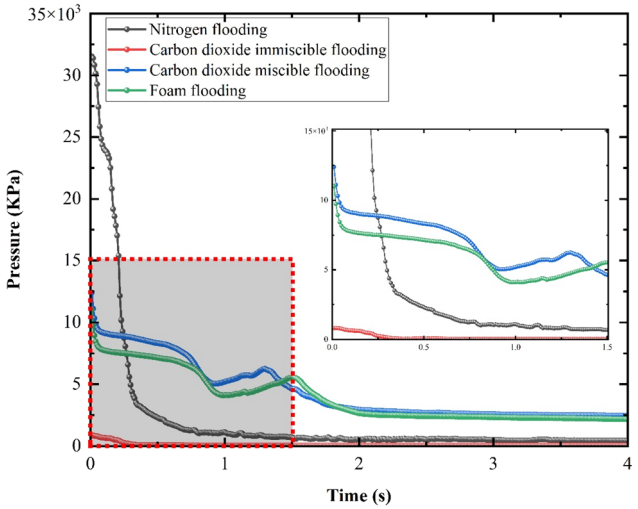

Fig. 27 Comparison of pressure changes with different gas flooding.

volume fraction diagram of remaining oil after oil flooding, it can be seen that the distribution of remaining oil is basically the same at different gas–liquid ratios, and most of the remaining oil is concentrated in the upper right part of the model. When the gas–liquid ratio is 4 : 1, a small part of crude oil in the lower part of the model is still not displaced out of the porous media. When the gas–liquid ratio is 3 : 1 and 1 : 1, the residual oil is only distributed in the upper right area of the model, and when the gas–liquid ratio is 3 : 1, the residual oil volume fraction is smaller. Therefore, we can get the best gas–liquid ratio of foam flooding is 3 : 1, and the oil recovery is the highest. It can be seen from Fig. 21 that the pressure change trend at the same point of the inlet with foam gas–liquid ratio of 4 : 1, 3 : 1 and 1 : 1 is basically the same, which gradually decreases to a certain value. The pressure at the beginning and end of the oil flooding process is basically the same. It can be seen that within a certain range, different foam gas–liquid ratio has little effect on the pressure at the inlet of the model.

It can be seen from Fig. 22 that the change trend of residual oil volume fraction with different foam gas–liquid ratio is roughly the same. From 0 s to 2 s, the decline rate of residual oil volume fraction is fast, and the oil flooding speed is fast during this period. From 2 s to 4 s, the decline rate of residual oil volume fraction is slow, and the oil flooding speed is slow. And at 4 s, when the foam gas–liquid ratio is 3 : 1, the remaining oil volume fraction is the smallest, and the remaining oil volume fraction is about 0.15. At this time, the oil flooding effect is the best. It can be seen that different foam gas–liquid ratio will have a certain impact on the oil flooding effect.

Under the condition that other initial conditions remain unchanged, the surface tension is changed for comparative simulation analysis. Under the initial conditions, two groups of models were added to change the surface tension to 0.02 N m^{-1} and 0.03 N m^{-1}, respectively. The oil flooding simulation is carried out for the three models, and the calculation results are shown in Fig. 23 below.

According to the calculation results, it can be seen that changing the surface tension has little effect on the overall pressure and fluid flow velocity. The pressure decreases

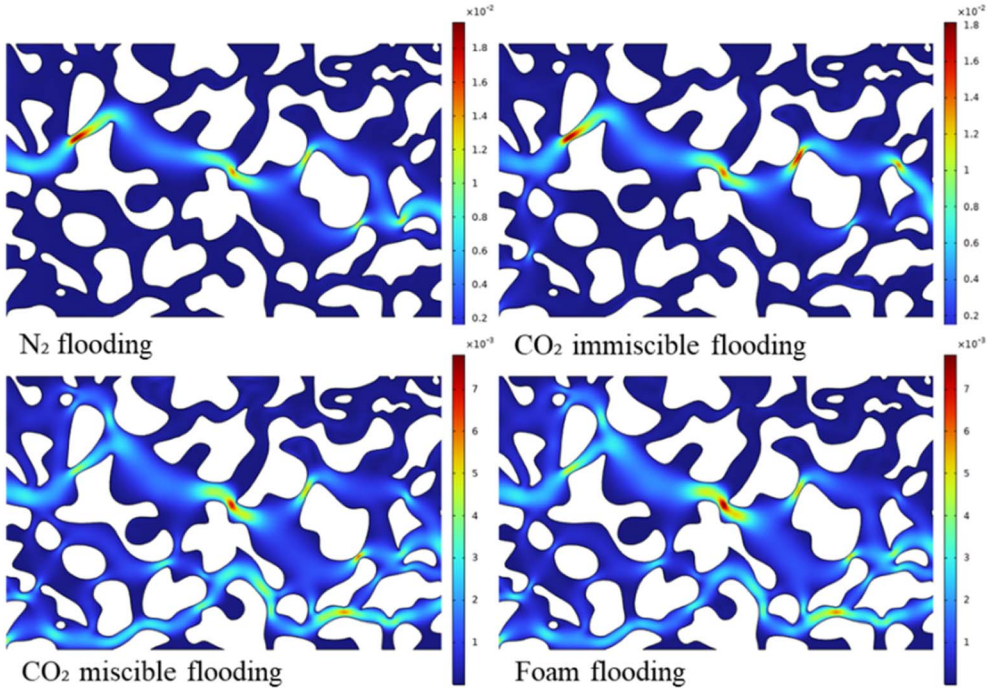

Fig. 28 Fluid flow velocity distribution with different gas flooding.

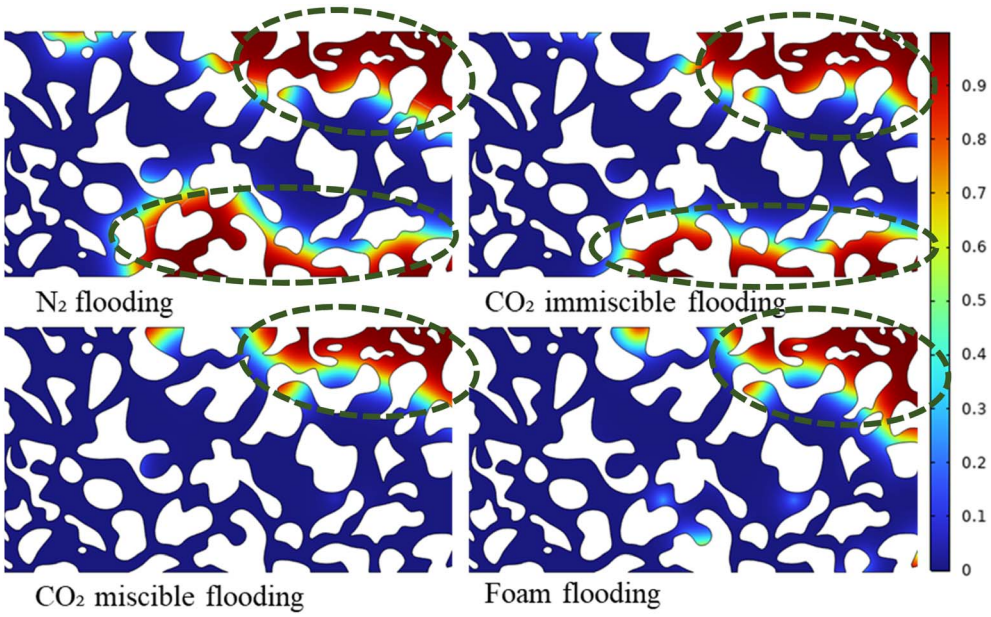

Fig. 29 Volume fraction distribution of remaining oil with different gas flooding.

gradually from the maximum near the inlet, and the fluid flow velocity is larger in some narrow channels. At the end of the oil flooding process, most of the remaining oil is concentrated in the upper right area of the model. When the surface tension is 0.01 N m^{-1}, compared with the other two groups of simulation results, there are still more crude oil residues in the lower middle area of the model. When the surface tension is 0.02 N m^{-1}, the volume fraction of remaining oil is smaller. Therefore, it can be concluded that the surface tension has a certain impact on foam flooding, and the oil recovery is higher when the surface tension is 0.02 N m^{-1}.

It can be seen from Fig. 24 that the pressure variation trend at the same point of the inlet with foam flooding surface tension of 0.01 N m^{-1}, 0.02 N m^{-1} and 0.03 N m^{-1} is basically the same, which gradually decreases to a certain value. The pressure at the beginning and end of the oil flooding process is basically the

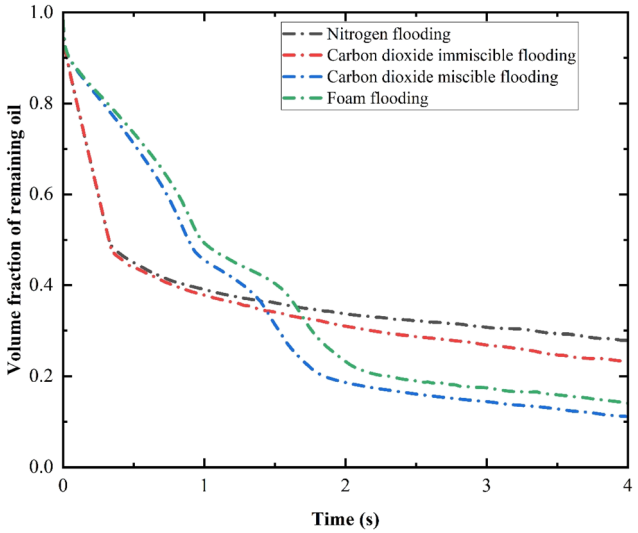

Fig. 30 Comparison of variation trend of residual oil volume fraction with different gas flooding.

same. At the 4th s, when the foam surface tension is 0.02 N m^{-1}, the pressure at this point at the inlet is the smallest. It can be seen that within a certain range, different foam surface tension has little effect on the pressure at the inlet of the model.

Fig. 25 shows that the change trend of residual oil volume fraction with different foam surface tension is roughly the same. From 0 s to 2 s, the decline rate of residual oil volume fraction is fast, and the flooding rate is fast. From 2 s to 4 s, the remaining oil volume fraction decreases slowly and the oil flooding speed is slow. When the foam surface tension is 0.02 N m^{-1}, the remaining oil volume fraction is the smallest, about 0.14, and the oil flooding effect is the best at this time. It can be seen that different surface tension of foam will have a certain impact on oil flooding effect.

Comparative analysis of different gas flooding

The initial conditions of the four kinds of gas flooding are set the same, and the injection rate is 0.001 m s^{-1}. Through comparative analysis, the pressure distribution at the same time is shown in Fig. 26 below.

It can be seen from Fig. 26 and 27 that although the types of gas flooding are different, the overall pressure decreases from left to right. The pressure near the inlet of the model is high, and the pressure near the outlet is small and close to 0 kPa. The difference is that at the beginning of oil flooding, the pressure of different types of gas flooding is nitrogen flooding, CO_2 miscible flooding, foam flooding and CO_2 immiscible flooding in descending order. At the end of oil flooding, the pressure is CO_2 miscible flooding, foam flooding, nitrogen flooding and CO_2 immiscible flooding in descending order.

As can be seen from Fig. 28, fluid flows in from the model inlet, flows from left to right, and flows out at the outlet. The distribution of N_2 flooding and CO_2 immiscible flooding in porous media is similar, and they are both distributed in the central channel of the model; The distribution of CO_2 miscible flooding and foam flooding in the model is close, and they are distributed in all parts of the model. The maximum flow rates of nitrogen flooding, CO_2 immiscible flooding, CO_2 miscible flooding and foam flooding are 0.025 m s^{-1}, 0.02 m s^{-1}, 0.008 m s^{-1} and 0.007 m s^{-1}, respectively. It can be seen that the flow velocity of fluid under different gas flooding is nitrogen flooding, CO_2 immiscible flooding, CO_2 miscible flooding and foam flooding in descending order.

According to the above initial conditions, continue to simulate and compare, and get the volume fraction distribution of the remaining oil on the surface at the same time, as shown in Fig. 29. It can be seen that the location distribution of the remaining oil in different gas flooding is different. The residual oil positions of nitrogen flooding and CO_2 immiscible flooding are similar, and they are concentrated in the upper part of the middle right and the lower part of the middle right, and both have more residual oil. The residual oil of CO_2 miscible flooding and foam flooding remains at the outlet and upper middle part of the model, but there is basically no residual oil in other areas of the model, and there is still a small amount of residual oil in the middle and lower part of the model after the end of foam flooding. The residual oil of these two oil flooding methods is less. The following Fig. 30 shows the variation trend of residual oil volume fraction for different gas flooding.

Fig. 30 shows that the curves of N_2 flooding and CO_2 immiscible flooding are relatively close, and the volume fraction of remaining oil is relatively large. It can be seen that under the same initial conditions, the crude oil recovery of these two oil flooding methods is poor, and the recovery effect of N_2 flooding is the worst, with the volume fraction of remaining oil of about 0.27, and the flooding efficiency is only 73%. The curves of CO_2 miscible flooding and foam flooding are relatively close, and the volume fraction of remaining oil is small. It can be seen that under the same initial conditions, the crude oil recovery of these two flooding methods is better, and the CO_2 miscible flooding has the best recovery effect, with the volume fraction of remaining oil about 0.1 and the flooding efficiency about 90%. In addition, in the early stage of the oil flooding process, N_2 and CO_2 immiscible oil flooding have faster oil flooding speed than the other two oil flooding methods, higher oil flooding efficiency and better early oil flooding effect, but as the oil flooding process enters the middle and late stage, the oil flooding speed becomes slow and gradually tends to be stable. CO_2 miscible flooding and foam flooding always maintain high oil flooding efficiency in the early and middle stages of oil flooding, and the oil flooding speed slows down and tends to be flat in the late stage of oil flooding process.

Conclusions

Based on the level set method, the mathematical model of gas flooding in porous media is established, and the reasonable initial conditions and fluid data are selected as simulation examples to simulate the oil flooding effects of N_2 flooding, CO_2 flooding, CO_2 miscible flooding and foam flooding on the micro scale. The previous work is large-scale research, and the geometric model based on it is usually some simplified models and conceptual models,[50–52] while the geometric model in this

paper is smaller, and it is based on the real core slice, which is closer to the reality. In addition, there have been many previous studies on single gas. This paper makes a comprehensive comparative analysis of several gases commonly used in oilfield development, which is more instructive. The main conclusions are as follows:

(1) The remaining oil volume fraction after nitrogen flooding is approximately 27%, *i.e.*, the oil displacement efficiency is around 73%. After CO_2 immiscible flooding, the remaining oil volume fraction is about 23%, corresponding to a displacement efficiency of roughly 77%. CO_2 miscible flooding results in a remaining oil volume fraction of approximately 10%, equating to a displacement efficiency of about 90%. Following foam flooding, the remaining oil volume fraction is around 14%, indicating a displacement efficiency of approximately 86%.

(2) Pressure variation curves during different gas displacement processes show that nitrogen flooding exhibits the highest inlet pressure and the fastest pressure drop rate. In contrast, CO_2 immiscible flooding has the lowest inlet pressure and the slowest pressure decline rate. The final inlet pressures for both nitrogen flooding and CO_2 immiscible flooding approach 0 kPa. The inlet pressures and their variation trends for CO_2 miscible flooding and foam flooding are similar, with their final pressures approaching 2.5 kPa.

(3) Velocity profiles for different gas displacement methods indicate that nitrogen flooding and CO_2 immiscible flooding have relatively lower flow velocities, with fewer regions of high flow rates. In comparison, CO_2 miscible flooding and foam flooding exhibit higher velocities and more extensive areas of high flow rates. The displacement effectiveness of nitrogen flooding and CO_2 immiscible flooding is relatively weaker, at about 70%, while CO_2 miscible flooding and foam flooding demonstrate better performance, achieving around 90% displacement efficiency.

(4) Increasing the injection rates of nitrogen, CO_2, and the CO_2-miscible phase can lead to improved early-stage displacement effects and a slight increase in recovery. Since this study treats foam as a single-phase fluid, simplifying its structural characteristics, the effects of surface tension and gas–liquid ratio on recovery were found to be insignificant.

Conflicts of interest

The authors declare that they have no known competing financial interests or personal relationships that could have appeared to influence the work reported in this paper.

Author contributions

Yi Yu: software, formal analysis, writing – original draft. Fei Wang: investigation, methodology, writing – reviewing and editing. Xiaorong Guo: validation, methodology. Chaofan Chen: resources, formal analysis. Yuqian Wang: data curation, methodology. Hailong Chen: validation, investigation.

Data availability

The data in this paper is mainly the simulation of software. The software used is COMSOL Multiphysics version 6.2. The geometric model (pore_scale_flow.mphbin) and simulation script (pore_scale_flow.mph) based on the simulation can be found at the following website: https://www.comsol.com/model/pore-scale-flow-488. The basic gas settings used in the simulation are given in Table 1, and other initial and boundary value conditions are also given in the paper. All simulation results are embedded in the content of the article in the form of pictures and charts.

Acknowledgements

This work was financially supported by the Shandong Provincial Natural Science Foundation (No. ZR2021QE008) and the Natural Science Foundation of Sichuan Province (No. 2024NSFSC0977) . We sincerely thank other persons in the Geo-Energy Research Institute for helping with the experimental research.

References

1 H. Wang, F. Ma, X. Tong, Z. Liu, X. Zhang, Z. Wu, *et al.*, Assessment of global unconventional oil and gas resources, *Pet. Explor. Dev.*, 2016, **43**(6), 925–940.
2 A. Bera, S. Kumar and J. Foroozesh, Multiphysics gas transport in nanoporous unconventional reservoirs: challenges of mathematical modelling, *J. Nat. Gas Sci. Eng.*, 2022, **103**, 104694.
3 Y. Song, Z. Li, Z. Jiang, Q. Luo, D. Liu and Z. Gao, Progress and development trend of unconventional oil and gas geological research, *Pet. Explor. Dev.*, 2017, **44**(4), 675–685.
4 Y. Zhao, D. Y. Zhao, R. Q. Zhong, L. R. Yao and K. K. Li, Research status and prospect of heavy oil recovery technology, *Key Eng. Mater.*, 2021, **888**, 165–172.
5 A. A. Adasani and B. Bai, Analysis of EOR projects and updated screening criteria, *J. Pet. Sci. Eng.*, 2011, **79**(1–2), 10–24.
6 B. V. Malozyomov, N. V. Martyushev, V. V. Kukartsev, V. S. Tynchenko, V. V. Bukhtoyarov, X. Wu, *et al.*, Overview of methods for enhanced oil recovery from conventional and unconventional reservoirs, *Energies*, 2023, **16**(13), 4907.
7 X. Liang, L. Shi, L. Cheng, X. Wang and Z. Ye, Optimization of polymer mobility control for enhanced heavy oil recovery: Based on response surface method, *J. Pet. Sci. Eng.*, 2021, **206**, 109065.
8 J. Yang and J. Hou, Experimental study on gas channeling characteristics of nitrogen and foam flooding in 2-D visualized fractured-vuggy model, *J. Pet. Sci. Eng.*, 2020, **192**, 107334.
9 X. Chen, Z. Yang, H. Yu, Z. Niu, W. Li, N. Jia, *et al.*, Enhancing oil recovery in low permeability reservoirs through CO_2 miscible flooding: mechanisms and dynamics, *ACS Omega*, 2024, **9**(50), 49336–49347.

10 Y. Fang, E. Yang, D. Yin and Y. Gan, Study on Distribution Characteristics of Microscopic Residual Oil in Low Permeability Reservoirs, *J. Dispersion Sci. Technol.*, 2019, **41**(4), 575–584.
11 W. Tang and J. J. Sheng, Huff-n-puff gas injection or gas flooding in tight oil reservoirs?, *J. Pet. Sci. Eng.*, 2022, **208**, 109725.
12 M. Ding, Y. Wang, D. Liu, X. Wang, H. Zhao and W. Chen, Enhancing tight oil recovery using CO_2 huff and puff injection: An experimental study of the influencing factors, *J. Nat. Gas Sci. Eng.*, 2021, **90**, 103931.
13 Z. Wu, Q. Feng, Y. Tang, D. Zhou and L. Lian, Experimental study on carbon dioxide flooding technology in the Lunnan Oilfield, Tarim Basin, *Energies*, 2024, **17**(2), 386.
14 R. Wang, W. Zhou, Y. Tang, D. Zhou, Z. Wu and L. Lian, Microscopic Experiments to Assess the Macroscopic Sweep Characteristics of Carbon Dioxide Flooding, *Appl. Sci.*, 2024, **14**(19), 9007.
15 E. Heidaryan and J. Moghadasi, A laboratory investigation into carbon dioxide flooding by focusing on the viscosity and swelling factor changes, *Pet. Sci. Technol.*, 2012, **30**(14), 1441–1452.
16 H. Han, X. Zhang, W. Zhang, Z. Li, L. Fan and C. Chen, Experimental study of asphaltene deposition as well as heavy oil recovery via CO_2 flooding, *J. Comput. Methods Sci.*, 2025, **25**(2), 1238–1245.
17 Z. Wu, Q. Feng, L. Lian, X. Meng, D. Zhou, M. Luo, *et al.*, Carbon dioxide oil repulsion in the sandstone reservoirs of Lunnan Oilfield, Tarim Basin, *Energies*, 2024, **17**(14), 3503.
18 J. Yang, J. Hou, M. Qu, T. Liang and Y. Wen, Experimental study the flow behaviors and mechanisms of nitrogen and foam assisted nitrogen gas flooding in 2-D visualized fractured-vuggy model, *J. Pet. Sci. Eng.*, 2020, **194**, 107501.
19 G. Feng, Y. Li and Z. Yang, Performance evaluation of nitrogen-assisted steam flooding process in heavy oil reservoir via numerical simulation, *J. Pet. Sci. Eng.*, 2020, **189**, 106954.
20 Y. Zhang, Y. Wang, F. Xue, Y. Wang, B. Ren, L. Zhang, *et al.*, CO_2 foam flooding for improved oil recovery: Reservoir simulation models and influencing factors, *J. Pet. Sci. Eng.*, 2015, **133**, 838–850.
21 D. Y. Ding, N. Farah, B. Bourbiaux, Y. S. Wu and C. Wang, Numerical simulation of low permeability unconventional gas reservoirs, in *SPE/EAGE European Unconventional Resources Conference and Exhibition*, 2014, p. D021S011R001.
22 J. Zhao, Development techniques of horizontal wells in low permeability reservoirs, Jilin Oilfield, *Pet. Explor. Dev.*, 2011, **38**(5), 594–599.
23 Y. Tian, O. Uzun, Y. Shen, Z. Lei, J. Yuan, J. Chen, *et al.*, Feasibility study of gas injection in low permeability reservoirs of Changqing oilfield, *Fuel*, 2020, **274**, 117831.
24 A. Das, N. Nguyen and Q. P. Nguyen, Low tension gas flooding for secondary oil recovery in low-permeability, high-salinity reservoirs, *Fuel*, 2020, **264**, 116601.
25 C. Zhang, P. Wang, G. Song, G. Qu and J. Liu, Optimization and evaluation of binary composite foam system with low interfacial tension in low permeability fractured reservoir with high salinity, *J. Pet. Sci. Eng.*, 2018, **160**, 247–257.
26 N. Ma, C. Li, F. Wang, Z. Liu, Y. Zhang, L. Jiang, *et al.*, Laboratory study on the oil flooding process in low-permeability cores with different injection fluids, *ACS Omega*, 2022, **7**(9), 8013–8022.
27 J. Luan, P. Dong and J. Zheng, Experimental studies on reaction laws during the process of air injection into the oil reservoirs with low permeability, *J. Pet. Sci. Eng.*, 2020, **194**, 107526.
28 F. Wang, Y. Zhang, Z. Yu and J. Chen, Simulation research on Jamin effect and oil displacement mechanism of CO_2 foam under microscale, *Arabian J. Chem.*, 2023, **16**(10), 105123.
29 F. Wang, D. Du, H. Bi, H. Wang, H. Chen and H. Li, Quantitative Characterization of Foam Transient Structure in Porous Media and Analysis of Its Flow Behavior Based on Fractal Theory, *Ind. Eng. Chem. Res.*, 2020, **59**(11), 5158–5166.
30 E. Manrique, C. Thomas, R. Ravikiran, M. Izadi, M. Lantz, J. Romero, *et al.*, EOR: current status and opportunities, in *SPE Improved Oil Recovery Conference*, 2010, p. SPE-130113.
31 W. L. Kang, B. B. Zhou, M. Issakhov and M. Gabdullin, Advances in enhanced oil recovery technologies for low permeability reservoirs, *Pet. Sci.*, 2022, **19**(4), 1622–1640.
32 A. Das, N. Nguyen and Q. P. Nguyen, Low tension gas flooding for secondary oil recovery in low-permeability, high-salinity reservoirs, *Fuel*, 2020, **264**, 116601.
33 J. Luan, P. Dong and J. Zheng, Experimental studies on reaction laws during the process of air injection into the oil reservoirs with low permeability, *J. Pet. Sci. Eng.*, 2020, **194**, 107526.
34 S. Yuan, Q. Wang, J. Li and H. Han, Technology progress and prospects of enhanced oil recovery by gas injection, *Acta Pet. Sin.*, 2020, **41**(12), 1623–1632.
35 Y. Jiang and B. Wang, A cost-effective method to enhance oil recovery of water-flooded reservoirs: air-foam flooding, in *SPE Asia Pacific Oil and Gas Conference and Exhibition*, 2013, p. SPE-165856.
36 W. J. O'Brien, R. G. Moore, S. A. Mehta, M. G. Ursenbach and M. I. Kuhlman, Performance of air injection vs. CO_2/water injection in a tight, light-oil reservoir: A laboratory study, *SPE Reservoir Eval. Eng.*, 2019, **22**(03), 1049–1062.
37 P. Pankaj, H. Mukisa, I. Solovyeva and H. Xue, Boosting oil recovery in naturally fractured shale using CO_2 huff-n-puff, in *SPE Argentina Exploration and Production of Unconventional Resources Symposium*, 2018, p. D033S012R001.
38 J. Guo, L. Ma and C. Lu, Progress and development directions of fracturing flooding technology for tight reservoirs in China, *Acta Pet. Sin.*, 2022, **43**(12), 1788–1797.
39 Y. Lu, X. Ao, J. Tang, Y. Jia, X. Zhang and Y. Chen, Swelling of shale in supercritical carbon dioxide, *J. Nat. Gas Sci. Eng.*, 2016, **30**, 268–275.
40 F. Wang, S. Ping, Y. Yuan, Z. Sun, H. Tian and Z. Yang, Effects of the mechanical response of low-permeability sandstone reservoirs on CO_2 geological storage based on

laboratory experiments and numerical simulations, *Sci. Total Environ.*, 2021, **796**, 149066.

41 C. Zhang, C. Yu, Z. H. Gu, K. Liu, P. K. Wu and Z. M. Li, Characterization and optimization of oil–gas interfacial tension during CO_2/N_2 injection in heavy oil reservoirs: Experimental study and regression model, *Pet. Sci.*, 2025, **22**, 2516–2534.

42 Z. Liu, J. Niu, Y. Guo, Y. Jia and M. Cui, Mechanisms of CO_2 enhanced gas recovery in tight-sand gas reservoirs, *Energy Geosci.*, 2025, **6**(2), 100393.

43 M. Auset and A. A. Keller, Pore-scale processes that control dispersion of colloids in saturated porous media, *Water Resour. Res.*, 2004, **40**(3), W03503.

44 S. Sirivithayapakorn and A. Keller, Transport of colloids in saturated porous media: a pore-scale observation of the size exclusion effect and colloid acceleration, *Water Resour. Res.*, 2003, **39**(4), 1255–1256.

45 A. Zolghadr, M. Escrochi and S. Ayatollahi, Temperature and composition effect on CO_2 miscibility by interfacial tension measurement, *J. Chem. Eng. Data*, 2013, **58**(5), 1168–1175.

46 M. S. Sanders and H. Chen, Supercritical CO_2 as an EOR agent: Its properties and roles in miscible displacement, in *SPE Improved Oil Recovery Symposium*, 2012, p. SPE-154122-MS.

47 V. Vesovic, W. A. Wakeham, G. A. Olchowy, J. V. Sengers, J. T. R. Watson and J. Millat, The transport properties of carbon dioxide, *J. Phys. Chem. Ref. Data*, 1990, **19**(3), 763–808.

48 A. Fenghour, W. A. Wakeham and V. Vesovic, The viscosity of carbon dioxide, *J. Phys. Chem. Ref. Data*, 1998, **27**(1), 31–44.

49 S. A. Khan and R. C. Armstrong, Rheology of foams: II. Effects of polydispersity and liquid viscosity for foams having gas fraction approaching unity, *J. Non-Newtonian Fluid Mech.*, 1987, **25**(1), 61–92.

50 C. Zhang, F. Wang, Z. Li and H. Chen, Dynamic simulation and experimental verification of foam transport in porous media based on level set method, *Energy Sci. Eng.*, 2019, **7**(1), 135–147.

51 F. Wang, D. Du, H. Chen and C. Zhang, Simulation of evolution mechanism of dynamic interface of aqueous foam in narrow space base on level set method, *Colloids Surf., A*, 2019, **568**, 25–33.

52 F. Wang, Z. Yu, J. Chen, Y. Yu and H. Chen, Dynamic simulation research on microprofile control mechanism of foam in fractured media based on level set method, *Langmuir*, 2024, **40**(20), 10816–10831.